IEEE Access
Multidisciplinary | Rapid Review | Open Access Journal

Received August 25, 2021, accepted September 13, 2021, date of publication September 28, 2021, date of current version October 19, 2021.

Digital Object Identifier 10.1109/ACCESS.2021.3116032

Fast Fault Detection Using Optimal Intrinsic Modes and Energy Deviation Matrix in Distribution Systems

NIEN-CHE YANG, (Member, IEEE), AND ABHILASH SEN
Department of Electrical Engineering, National Taiwan University of Science and Technology, Taipei 10607, Taiwan

Corresponding author: Nien-Che Yang (ncyang@mail.ntust.edu.tw)

This work was supported in part by the Ministry of Science and Technology (MOST), Taiwan; in part by MOST under Grant MOST 109-3111-8-011-001; and in part by the DELTA-NTUST Joint Research Center.

ABSTRACT The detection, classification, and location of grid faults have always been challenging for power engineers. Among these, the detection of the grid fault is the most critical task because, without the detection, the remaining two processes will not start. In this study, a fast light-weight fault detection is proposed. This technique uses an empirical mode decomposition to decompose the fault signals into intrinsic mode functions (IMFs). Effective IMFs were selected using the earth mover's distance-based selection algorithm. The selected IMFs are then passed through an energy calculator and then through a moving median absolute deviation stage to generate an energy deviation matrix (EDM). Based on the EDM, the occurrence of faults can be determined. The proposed technique was verified by evaluating various grid fault scenarios using the MATLAB/Simulink software platform. Furthermore, the proposed method shows a more precise and satisfactory performance than existing standard fault-detection methods.

INDEX TERMS Earth mover's distance, empirical mode decomposition, fault detection, median absolute deviation, optimal intrinsic mode functions, radial distribution system.

I. INTRODUCTION

Power outages, also known as blackouts, are the worst-case scenarios that can be encountered by a utility grid. The world has already experienced significant blackouts in the past [1]. The diffusion of renewable energy sources, integration of dynamic industrial loads, and the increase in distributed generation (DG) affect the distribution network parameters, which may increase the risk of power failures [2]. The results of relevant analysis and research show that a simple electrical fault can cause a blackout in a distribution system [3]–[5]. For this reason, power system engineers have analyzed the electrical fault characteristics throughout the last decade.

The first step of an electrical fault analysis always starts with fault detection. Other investigations, even if fundamental, were carried out at later stages. Over the last few years, several researchers have contributed to fault detection. In [6], satisfactory results were obtained using a wavelet-transform-based detection technique. However, the mother wavelet selection remains a problem because the selection criteria depend on data and network models. Similarly, Guillen *et al.* [7] proposed a reliable fault-detection index using a wavelet covariance matrix and power spectral density. To make the detection process fast but simple, Li *et al.* [8] used the rate of change of current as the principal detection criterion. However, this method requires a high sampling frequency to detect small variations. Furthermore, noise interference may affect the overall performance of detection algorithms. In [9], Guo *et al.* proposed a current-limiting method based on the variation of the area under the curve technique. The area under half cycles was recorded, and the standard deviation was used to detect unexpected variations in the distribution system. In [10], a high-impedance fault detection method was proposed in the presence of nonlinear loads. The Stockholm transform was used to extract the information related to the 3rd harmonic component to detect the fault in a distribution system. However, harmonic-based detection techniques are often threatened by noise and switching of electronic components. In [11], a cyclo-stationary characteristic-based detection method was proposed. Cyclic

The associate editor coordinating the review of this manuscript and approving it for publication was Mehrdad Saif.

autocorrelation information is extracted from the fault signal and compared with the predefined fault templates. Although the detection results were accurate, the computational complexity was $2N^2$, which is large for detection algorithms. In [12], a distortion-based fault-detection technique was proposed. The distortions of the fault signals are extracted using the Grubbs criterion-based linear least square criterion and compared with predefined values. Similarly, in [13], the angle between the zero-sequence voltage and the current phasor was used as the driving point of the fault detection algorithm.

Tsiafis *et al.* [14] used empirical mode decomposition (EMD) and spectral analysis to detect faults in ball bearings in a rather innovative way. Jiang *et al.* [15] proposed a technique for detecting faults in rotating machines. The ensemble EMD (EEMD) was used to decompose the fault signals, and then the cloud-modeled bi-spectrum analysis to detect the faulty case. In [16], EMD was used to decompose the fault current signals into a series of generated intrinsic mode function (IMF) signals. A Hilbert-Huang transform filter is then used to extract critical features and detect faults. The methods mentioned above involving EMD-IMFs can be improved by using the IMF selection algorithm. With the recent development of signal processing techniques, such as EMD and EEMD, extensive applications in other fields require research on IMF selection.

In signal processing, the selection of IMFs has been used carefully. Cho *et al.* [17] introduced a power-harmonic ratio (PHR) as an index for selecting the critical IMFs of a given signal. In addition, faulty signals may have more power/energy and harmonic content. The higher the PHR ratio, the higher is the importance of the IMFs. Often, normal operations may cause significant amplitude variations and introduce harmonic components. In [18], a selection algorithm based on cross-correlation was proposed. The cross-correlation of all the IMFs with the original signal determines the point of discrimination. Kumar *et al.* [19] used the dynamic time warping (DTW) technique as a similarity detection platform for IMFs. However, DTW may contain several problems in alignment, time ordering, and maximum value pairing [20]. Considering all these factors, the contributions of this study are as follows.

1) The proposed effective selection of IMFs was performed using the earth mover's distance (ErMD).
2) A fast and reliable moving median absolute deviation (MAD)-based fault detection method was proposed using the EMD-IMF concept.

The Remainder of This Paper Is Organized as Follows: Section II introduces the optimum IMF selection algorithm and provides insight into the ErMD method. Section III describes the proposed fault-detection method. Section IV presents the results obtained using the proposed method. Finally, Section V presents our conclusions and references.

II. OPTIMUM IMF SELECTION ALGORITHM

This section emphasizes the proposed IMF selection method. In this study, ErMD was used as the similarity measure. The following subsections present the ErMD with some modifications to satisfy current applications.

A. EARTH MOVER'S DISTANCE (ErMD)

In 2000, Rubner *et al.* introduced the term ErMD and used it in image retrieval technology [21]. Initially, it was presented as an excellent method for calculating the similarity between two distributions in space. Later, ErMD was used for probability distributions [22], histogram comparisons [23], and audio and video processing [24]. For any given two distributions, a_k and b_l, the ErMD is defined as [21]:

$$\text{ErMD} = \frac{\sum_{i=1}^{k}\sum_{j=1}^{l} d_{ij}\, p_{ij}}{\sum_{i=1}^{k}\sum_{j=1}^{l} p_{ij}}, \tag{1}$$

where d_{ij} represents the distance between a_i and b_j (often standard distance evaluation methods are adopted), and p_{ij} represents the corresponding probability values.

According to the ErMD presented above, it is evident that the effective IMF selection problem cannot be addressed directly. Some fundamental differences are as follows: (a) ErMD was used for many-to-many alignments. In this case, each element of a_k connects with the corresponding element of b_l. Thus, a one-to-one alignment is required to solve this problem. (b) ErMD is efficient for probability distributions. However, this problem concerns time-series data, and (c) the dimensions of both distributions are different. In our case, the data streams were of the same size. For these reasons, the current ErMD must be modified to solve the IMF selection problem. After including the modifications in (1), as mentioned above, the modified ErMD* is expressed as follows:

$$\text{ErMD}^* = \frac{\sum_{i,j=1}^{k} d_{ij}\, p_{ij}\, s_{ij}\, e_{ij}}{\sum_{i,j=1}^{k} p_{ij}}, \tag{2}$$

where d_{ij} and p_{ij} represent the distance between a_i and b_j and the corresponding probability values, respectively. The total length is k for both the distributions. The two terms s_{ij} and e_{ij} are included, which represent the differences in stiffness and energy, respectively.

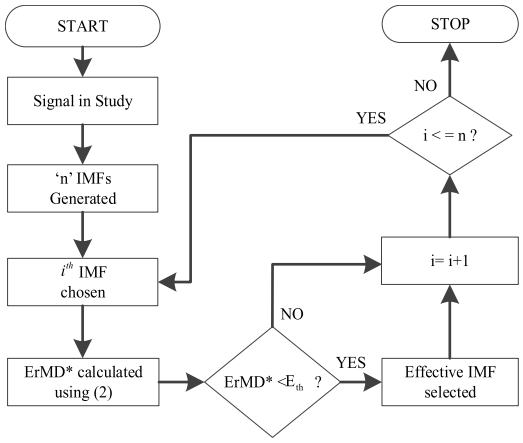

FIGURE 1. Flowchart of the proposed IMF selection algorithm.

B. PROPOSED IMF SELECTION METHOD

A flowchart of the proposed method for calculating the threshold limit, E_{th}, and ErMD* for a given signal is shown in Fig. 1. The signal is decomposed using EMD and generates the corresponding IMFs. The iterative cycle starts with the first IMF. The similarities between the IMF and the original signal were calculated using ErMD*. The lower the ErMD* value, the better the IMF approximates the original signal. The calculated ErMD* was compared with the minimum threshold limit, E_{th}. An IMF is considered optimal when ErMD* is less than E_{th}.

Equation (2) was used to calculate the distance between the IMF and the original signal. Here, d_{ij} represents the Euclidean distance between the points of the original signal, and the IMF is at a fixed time. p_{ij} represents the probability 1/N, where N is the total number of data points; s_{ij} represents the stiffness difference between two adjacent point pairs in the original signal and IMF the signal at specified time intervals; and s_{ij} is used to study the previous and following trajectories of the waveforms. Similarly, e_{ij} represents the energy difference of three consecutive points, denoted by m^{th}, $(m-1)^{th}$, and $(m+1)^{th}$, of the two signals at specified time intervals. The threshold E_{th} is obtained by considering the energies and the total number of IMFs. The threshold E_{th} was calculated as follows:

$$E_{th} = \frac{1}{n} \sum_{i=1}^{n} \sum_{j=1}^{N} |u_i(j)|^2, \tag{3}$$

where $u_i(j)$ represents the value of a data point in the i^{th} IMF in the interval j, N is the total number of data points, and n is the total number of IMFs.

III. PROPOSED FAULT DETECTION TECHNIQUE

Independent of the fault types and conditions, the line currents always reflect the fault characteristics. In particular, the zero-and negative-sequence components of the currents contain partial information about the faults. These components were also considered in the proposed method. In Fig. 2, the complete fault detection process is explained through a flowchart. The three-phase currents on the secondary side of the main transformer were recorded. Furthermore, the zero- and negative-sequence components were obtained through a symmetrical component transformation.

A. GENERATION OF INTRINSIC MODE FUNCTION

Signal processing techniques have always been used to analyze any signal. In this study, EMD is used to decompose the signal into IMFs based on the local characteristics of the signal. The IMFs are extracted from the original signal so that higher-frequency components are filtered out first. Eventually, the last IMF contains the lowest frequency component in the signal. In the proposed method, the EMD-IMF is used to analyze the fault signals on a frequency scale. Since a fault may generate high-frequency current transients with non-stationary signals, the main fault characteristics lie within the first to 2-3 IMFs. Additionally, the EMD-IMF also

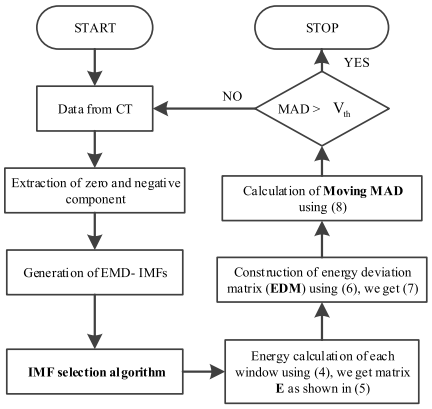

FIGURE 2. Flowchart of the proposed fault detection method.

acts as a noise remover, which is impossible if a simple high-frequency filter is used. In the first step, EMD [25] is used to decompose the signals into their corresponding modes, also known as IMFs. All the mode functions obtained have the same zero-crossing index numbers and are symmetric with respect to the zero-local means. The generation of IMFs is based on two factors: (1) the "local extrema" counts in a time series shall be the same or differ by one respect to the number of zero crossings and (2) the "local mean" surrounded by minima and maxima shall be zero at all points [26]. The first and second factors ensure a "global objective" and "local objective," respectively. The iterative process starts by generating the upper and lower envelopes based on local maxima and minima, respectively. If the above two conditions are satisfied, the obtained signal is considered an IMF. If the conditions are not satisfied, the means of both the lower and upper envelopes are subtracted from the original signal, and the iterative cycle repeats.

At the end of the process, all the IMFs are aligned. The selection of optimal IMFs is implemented using (2) and (3), as explained in Section II. The selected IMFs are merged, resulting in filtered signals that are later forwarded to the energy deviation matrix stage.

B. CONSTRUCTION OF ENERGY DEVIATION MATRIX

The filtered zero and negative sequence components are arranged in a matrix W, assuming that the two components have K data points. Each element in the matrix is indicated as W_{ij} (where $i = 1, 2$ represents two rows for two signals and $j = 1, 2, \ldots,$ K). Data points were divided into equal interval groups. If each group contains the same number of data points F, there are in total H = K/F groups. The energy E_{ih} of each group was calculated using (4).

$$E_{ih} = \sum_{m=1}^{F} |c_{ih}(m)|^2 \, \Delta t, \tag{4}$$

where c_{ih} (m) is the amplitude of the data points at m, in group h, and for signal i, and Δt is the sampling period. In this case, the sampling frequency was fixed at 10 kHz. The parameters were defined as follows: K = 200, F = 10, and H = 20. In other words, 200 data points were divided into 20 groups,

with 10 data points in each group. After evaluating the energy of all groups, the energy matrix **E** is defined as follows:

$$\mathbf{E} = \begin{bmatrix} \mathbf{E}_1 \\ \mathbf{E}_2 \end{bmatrix} = \begin{bmatrix} E_{11} & E_{12} & \cdots & E_{1h} \\ E_{21} & E_{22} & \cdots & E_{2h} \end{bmatrix}, \tag{5}$$

The standard deviation (SD) is suitable for variation measurements. However, when the evolution of the problem is unpredictable, SD is not the best choice. Given that the SD shows squared errors, minor disturbances may appear to be significant. In this study, the median absolute deviation (MAD) was used. To analyze the variations between the points more precisely, a moving MAD was used with a window of 4. The energy deviation matrix (EDM) is obtained by applying the MAD to matrix E using (6). The final moving MAD value is obtained by summing the components of the EDM, as shown in (8). Subsequently, this value was compared with the fault-detecting threshold V_{th}.

$$\begin{aligned} \mathbf{EDM} &= mad\,[\mathbf{E}] \\ &= \begin{bmatrix} median\,(|\mathbf{E}_1 - median\,(\mathbf{E}_1)\,|) \\ median\,(|\mathbf{E}_2 - median\,(\mathbf{E}_2)\,|) \end{bmatrix}, \end{aligned} \tag{6}$$

$$\mathbf{EDM} = \begin{bmatrix} E_Z \\ E_N \end{bmatrix}, \tag{7}$$

$$Moving\ MAD = [E_Z + E_N], \tag{8}$$

where E_Z and E_N are the zero-and negative-sequence components of the energy deviation matrix, respectively.

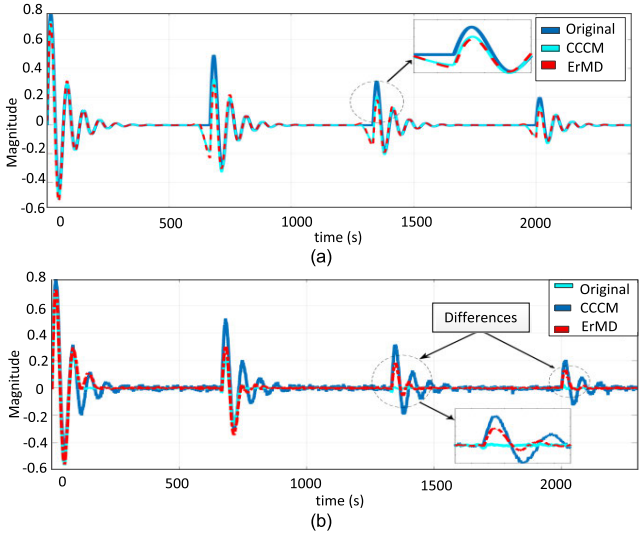

FIGURE 3. Original signal along with the final output from both methods: (a) without noise and (b) with the noise of SNR 20.

IV. RESULTS AND DISCUSSION

A. RESULTS OF OPTIMUM IMF SELECTION

In this section, the proposed optimum IMF selection algorithm is evaluated. The proposed method was compared with the standard cross-correlation coefficient method [27], and the results are presented in Fig. 3. Two signal scenarios were adopted for testing: the first input signal was the induction motor bearing vibration data with an inner race fault [28], and the second input signal was a train of custom pulses generated by the MATLAB environment. Table 1 shows the IMF selection outputs obtained via the proposed earth mover's method (ErMD*) and cross-correlation coefficient method (CCCM). It is observed that, owing to the ErMD* threshold limit, more IMFs were selected than those of the conventional CCCM.

TABLE 1. Selection of optimal IMFs.

Signal	ErMD IMF selection	CCCM IMF selection
Bearing vibration signal (Total IMFs-8)	IMF 1 IMF 2 IMF 3	IMF 2
Train of pulses without noise (Total IMFs-4)	IMF 1	IMF 1
Train of pulses with noise (Total IMFs-7)	IMF 4 IMF 5	IMF 5

Therefore, the proposed method can efficiently approximate the original signal while maintaining its main features. Fig. 3 (a) shows that both CCCM and ErMD are adequate for approximating the original signal. However, Fig. 3(b) shows that when the original signal contains white Gaussian noise with a signal-to-noise ratio (SNR) of 20, the CCCM cannot detect the spikes of the original signal, whereas the ErMD shows reliable performance.

B. RESULTS OF FAULT DETECTION ALGORITHM

To verify the feasibility of the proposed fault-detection algorithm, some scenarios were considered. A 10 kV solidly grounded distribution system was modeled using the MATLAB software platform, as shown in Fig. 4. A 110 kV/10 kV delta (Δ)- grounded star (Yg) transformer was connected to the main bus-bar of 10 kV. The model network and parameters in [6] were adopted, with some minor modifications.

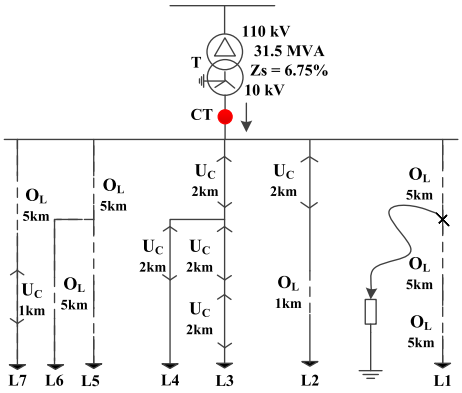

FIGURE 4. Schematic showing the distribution system under study.

The sampling time of the simulation was 10 kHz. The conductors were defined using a three-phase pi-section model. The overhead lines (O_L) and underground cables (U_C)

TABLE 2. Variable parameters of cables.

Parameters per km	Underground Cables (U_C)	Overhead Lines (O_L)
R_0 (Ω)	2.70	0.28
R_1 (Ω)	0.27	0.13
C_0 (μF)	0.28	0.06
C_1 (μF)	0.34	0.01
L_0 (mH)	1.02	4.60
L_1 (mH)	0.26	1.30

where subscript '0' denotes zero-sequence parameters, and subscript '1' denotes positive-sequence parameters.

are discriminated using the different parameters presented in Table 2 and 3. The receiving end of each line $L_i (i = 1, 2, \ldots, 7)$ has a constant power load of $0.5+j0.25$ MVA. All disturbances were introduced in L_1 at a distance of 5 km from the main bus. A current transformer (CT) was used to measure the current flowing through the main bus. The threshold value for the moving MAD was set to 200. It is worth mentioning that the choice of threshold limit is made considering the reliability and swiftness. Lower threshold values can definitely ensure swiftness, but it may not be reliable because it may detect a normal case as a faulty one. In contrast, higher threshold values guarantee reliability, but the overall process may become slow. In this case, reliability is preferred over swiftness.

TABLE 3. Parameters of test system.

Equipment	Ratings
3 phase transformer (Dyn11)	31.5 MVA, 110 kV-10 kV, 50 Hz
3 phase pi-section model	Length- 2 km,5 km
Non-linear load	0.5+0.25 MVA

1) LOW-RESISTANCE SINGLE LINE-TO-GROUND SHORT-CIRCUIT FAULT

A low-resistance fault ($R_f = 1\ \Omega$) is introduced in L_1 at a distance from the main bus of 5 km, in phase "a." The fault inception angle (FIA) is varied from 0° to 150° in steps of 30°. Fig. 5 shows the detection results obtained with a low-resistance single-line-to-ground fault.

It is observed that, given that the phase current amplitude increases rapidly, there are considerable fluctuations in the zero-and negative-sequence components. As a result, the energy deviation method can detect the fault in approximately 1.4 ms. Additionally, the performance of the proposed method under different FIAs, such as 0°, 30°, 60°, 90°, 120°, and 150°, is presented. The results show an adequate fault-detection time. The fastest detection time is achieved when FIA = 150° and slowest when FIA = 120°. However, single-phase low-resistance faults can be detected by the proposed method within 2 ms.

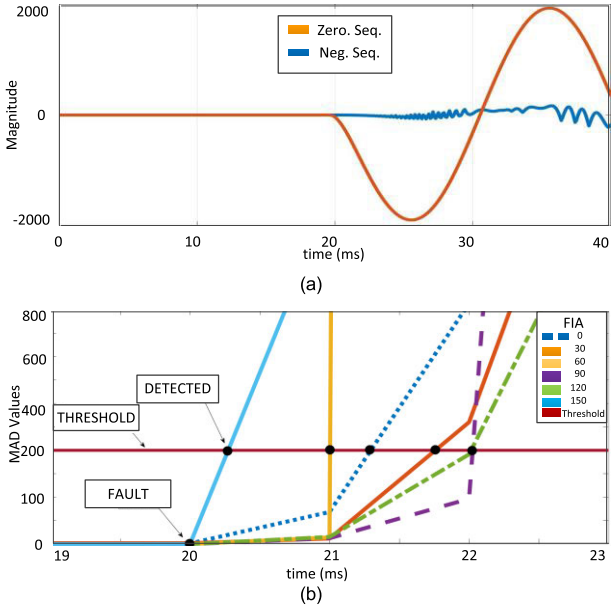

FIGURE 5. Low-resistance single-line-to-ground fault: (a) zero and negative sequence components and (b) MAD for different FIAs.

2) HIGH-RESISTANCE SINGLE LINE-TO-GROUND SHORT-CIRCUIT FAULT

Typically, it is difficult to detect high-resistance faults because the peak current in the faulty phase is difficult to detect. As a result, the behavior of this test case is very similar to the normal variations in the distribution systems. A single line with a high resistance ($R_f = 100\ \Omega$) fault is introduced in phase "a" of L_1. Fig. 6 shows the detection results obtained for a high-resistance single-line-to-ground fault.

The peak current in the faulted phase is lower than that obtained in the previous test case using a low resistance (see Fig. 6 (a)). If the fault resistance is increased further, a high similarity with a transformer inrush or even unbalanced operating conditions can be found. Compared with the previous case, the maximum fault detection time obtained with FIA = 150° is approximately 2.7 ms (see Fig. 6 (b)), while the maximum detection time was 2 ms for the low-resistance fault case.

3) DOUBLE LINE SHORT-CIRCUIT FAULT

Maintaining the fault location constant, a solid double line short-circuit fault between phases "a" and "b" is introduced. Fig. 7 shows that the current spikes after and before the fault allow the proposed detection algorithm to perform faster. This clearly shows the increased amplitude of the two faulted phases. Fig. 7 (a) shows that the amplitude of the pre-fault current is zero; however, it is not. The similar performance obtained for all the FIAs reduces the maximum fault detection time to 1.4 ms, with 150° as the slowest and 30° as the fastest detected cases (Fig. 7 (b)).

In addition, a low-resistance ($R_f = 1\ \Omega$) double-line short-circuit fault was introduced while leaving the other conditions

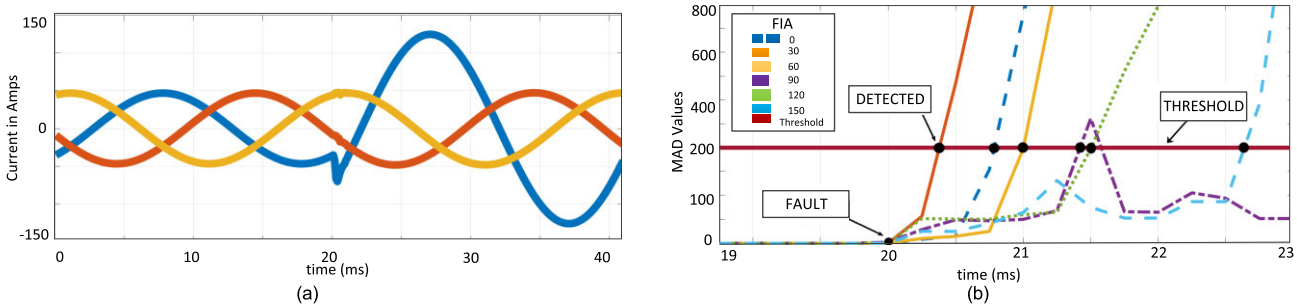

FIGURE 6. High-resistance single-line-to-ground fault: (a) three-phase line current and (b) MAD for different FIAs.

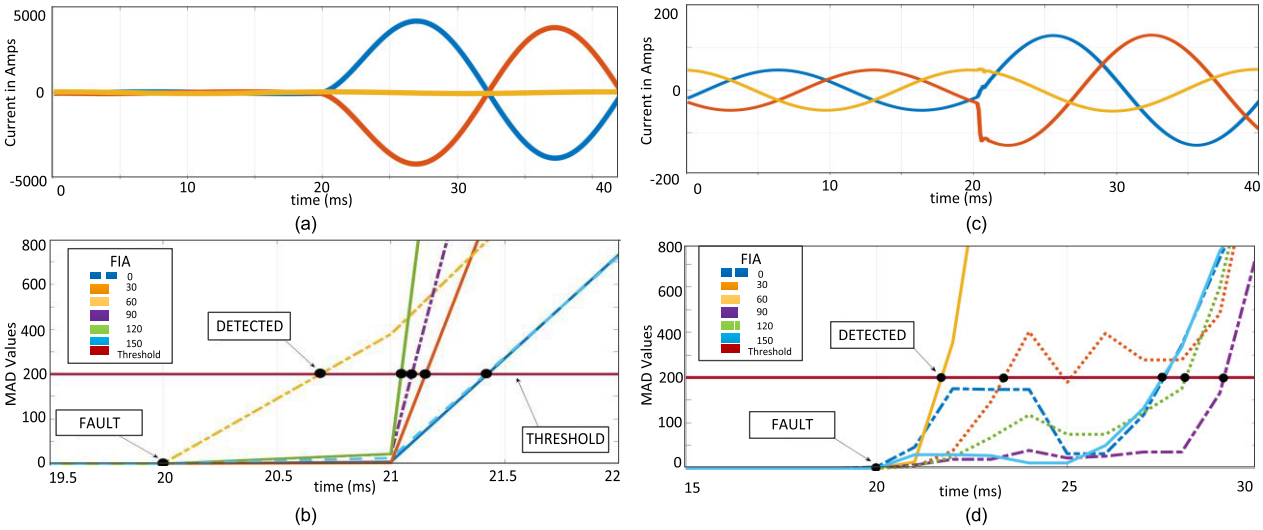

FIGURE 7. Double phase fault detection: (a) three-phase line current during low resistance fault, (b) MAD for different FIAs for low resistance fault, (c) three-phase line current during high resistance fault, and (d) MAD for different FIAs under high resistance fault.

unchanged. The characteristics of the low-resistance short-circuit faults and solid double-line short-circuit faults are similar. Owing to the limitations on the paper length, the results of the low-resistance short-circuit faults are not presented. Therefore, only solid short-circuit faults have been considered.

Fig. 7 (c) shows the three-phase line currents during the high-resistance double line to the ground fault. The performance of the proposed method for different FIAs is shown in Fig. 7 (d). The results show a considerable difference in the fault current peaks owing to an increased fault resistance. The effect of the peak fault currents on the fault-detection time was also significant. For this test case, the fastest and slowest fault-detection times were 2 ms and 8 ms, respectively.

4) SYMMETRICAL THREE-PHASE FAULT

Symmetrical three-phase faults are the most critical owing to their high peak fault currents. The balanced nature after a fault also holds a challenge in fault detection schemes. A solid three-phase fault was introduced in L_1. Fig. 8 shows the large peak of the post-fault current. Fig. 8 (a) shows that the considerable fault current and its negative sequence component allow the proposed fault detection method to operate quickly. In particular, 10 ms after the fault occurred, the negative sequence current became zero again, making this fault difficult to detect. The fault-detection time varied between 1 ms and 3 ms for different FIAs (Fig. 8 (b)).

5) OPEN CIRCUIT FAULT

Open circuit faults are uncommon. However, these are discussed in this paper. In particular, we considered the conductor fault that occurs at the end of L_1 at FIA $= 0°$, using phase ''a'' as a reference.

Fig. 9 shows the simulated results of open-circuit faults. When an open-circuit fault occurs, the faulted phase current decreases significantly and ideally reaches zero. As a result, a difference between the levels is generated, and the MAD of the predefined threshold increases. The proposed method detects the presented fault case in approximately 22 ms, which is relatively fast for an open-circuit fault in a 50 Hz system.

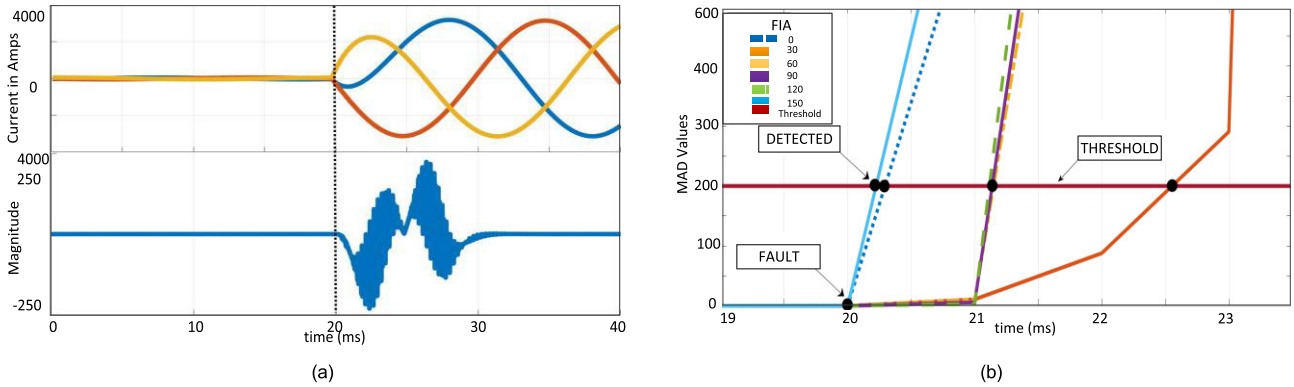

FIGURE 8. Solid three-phase fault: (a) three-phase current and negative sequence component and (b) MAD for different FIAs.

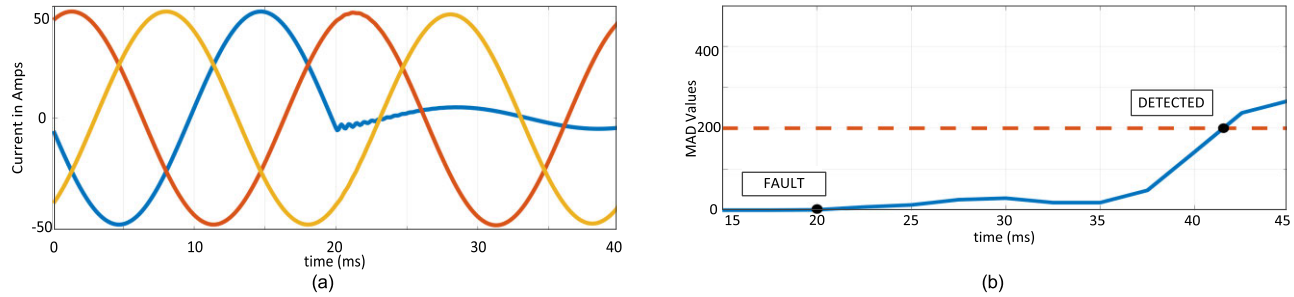

FIGURE 9. Open circuit fault in phase "a": (a) three-phase line current and (b) MAD for FIA = 0°.

6) TRANSFORMER INRUSH CURRENT

The normal conditions that appear to be faulty must be verified to confirm the reliability of the proposed detection method, and the transformer inrush current problem is one of them. The distribution transformers undergo various turning on and off states. In the restarting process, the machine may supply a transient current that is approximately 15–20 times higher than the rated current. However, this process is considered to be a normal operating state. Fig. 10 shows the performance of the proposed detection method when an inrush current occurs. The current causes a significant transient fluctuation (Fig. 10 (a)), and the moving MAD reaches a value between 20 and 30, which is still quite low compared to the predefined threshold of 200 (Fig. 10 (c)).

7) LOAD DEVIATION

In distribution networks, sudden load deviations are common and unpredictable. As a result, they can affect the performance of fault detection methods. Fig. 10 (c) shows the MAD when sudden load deviations of 10% and 20% occur in the distribution system. It was observed that the MAD was much lower than the predefined threshold, avoiding any false alarm.

8) VOLTAGE IMBALANCE

Unbalanced problems in power grids remain a challenge for power engineers. They are often caused by unbalanced three-phase loads in distribution systems. The International Electrotechnical Commission [29] recommends maintaining voltage imbalances below 2%, while the national electrical manufacturers association [30] considers a voltage imbalance of 1% safe for operations. In general, the current imbalance is 5–10 times higher than the voltage imbalance [31]. In this test case, a voltage imbalance of 1% was introduced in phase "a" at 20 ms, which resulted in a current imbalance of 5%, as shown in Fig. 10 (b). The moving MAD shows variations that are much lower than the predefined threshold of 200. However, a high percentage of voltage and current imbalance may be similar to high-impedance fault conditions. In this case, the possibility of having a false detection alarm is high and requires variations in the predefined threshold.

9) FAULT DURING UNBALANCED STATE

Typically, a small proportion of the unbalanced component exists in the utility grid. Further, a single-phase to ground fault is introduced during a voltage imbalance of 1%, as depicted in Fig 11. At 20 ms, a voltage imbalance of 1% was introduced in the distribution system. As a result, the moving MAD shows values that are much less than the predefined threshold. At 60 ms, a single-phase high-resistance fault was introduced into the power grid. Consequently, the MAD reaches a threshold limit of 200, as shown in Fig. 11. It is also worth mentioning that the system performance might overlap with the fault characteristics if the imbalance increases further. However, the performance of the proposed method

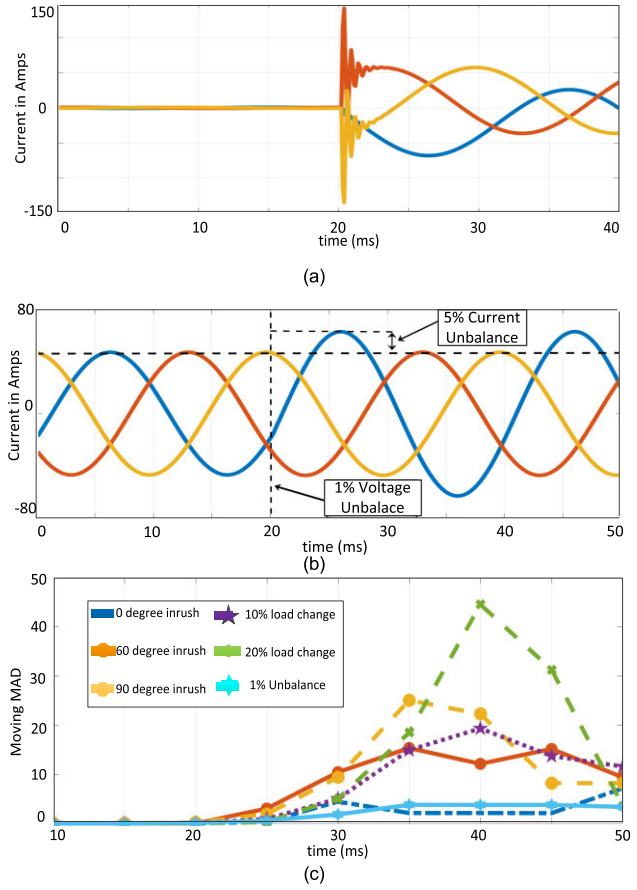

FIGURE 10. Normal conditions: (a) three-phase line current during transformer inrush, (b) three-phase line current during voltage imbalance = 1%, and (c) MAD for different cases.

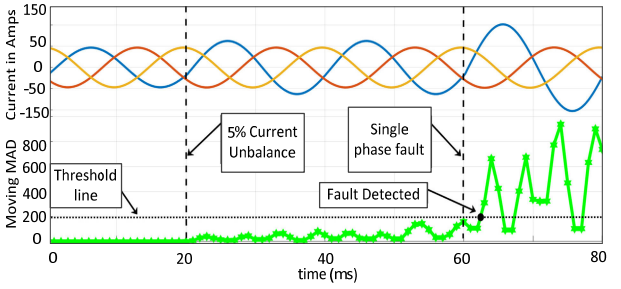

FIGURE 11. Three-phase line current and MAD for single-phase fault during voltage imbalance = 1%.

might be improved by modifying the predefined threshold limit.

10) ANTI-INTERFERENCE CAPABILITY

In realistic situations, the voltage and current signals may include noise that could affect fault detection. To test this possibility, white Gaussian noise with a SNR of 20 was added to the current signals, as shown in Fig 12. As a result, the presence of noise in the zero sequence and negative sequence components is inevitable. A single line-to-ground fault is

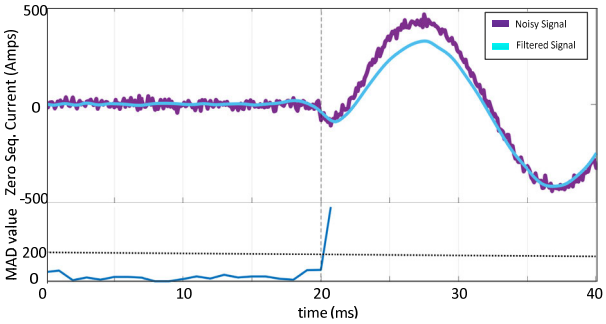

FIGURE 12. EMD-IMFs of zero sequence component during single line-to-ground fault.

adopted in phase "a". When a noisy element is present, the proposed IMF selection algorithm can be used to improve the performance of the fault detection algorithm. The noisy zero-sequence current component was filtered and smoothed to maintain the signal fluctuations intact. Hence, the fault-detection time of the proposed algorithm is not significantly affected by the introduction of a noisy element. Furthermore, decreasing the SNR may cause the output signal to lose its original information.

11) NETWORK TOPOLOGY

In fault detection methods, any network change is perceived as a challenge. In view of this, the topology of the sample network was modified in this study. Initially, the distribution network was a radial system arrangement, as shown in Fig. 4. Here, the feeders L1 and L2 are tied via a common bus, and a single load is tapped off the common bus. The modified distribution network is presented in Fig. 13 as a hybrid radial-meshed distribution network. Various line faults were introduced at the load-end side. The simulation results are listed in Table 4.

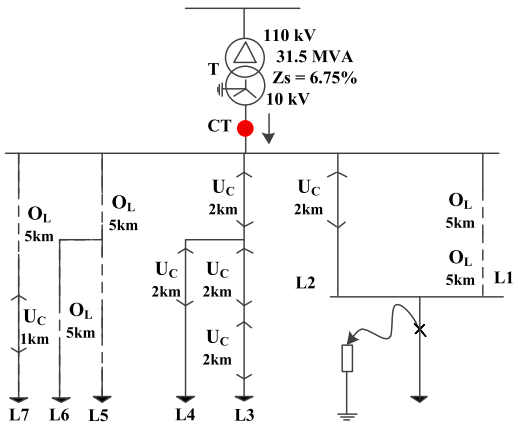

FIGURE 13. Modified distribution network with feeders L1 and L2 tied via a common bus.

The fault transients at the main bus were not significantly affected, due to the network topology characteristics. The waveform shape and the behavior of the sequence currents

TABLE 4. Fault detection times for various fault cases.

Fault cases	Radial network (ms)	Hybrid network (ms)
Single line-to-ground low-impedance fault	1.3	1.1
Single line-to-ground high-impedance fault	0.9	1.2
Double line-to-ground low-impedance fault	1.5	1.8
Double line-to-ground high-impedance fault	1.5	1.8
Solid triple line-to-ground fault	0.3	0.9

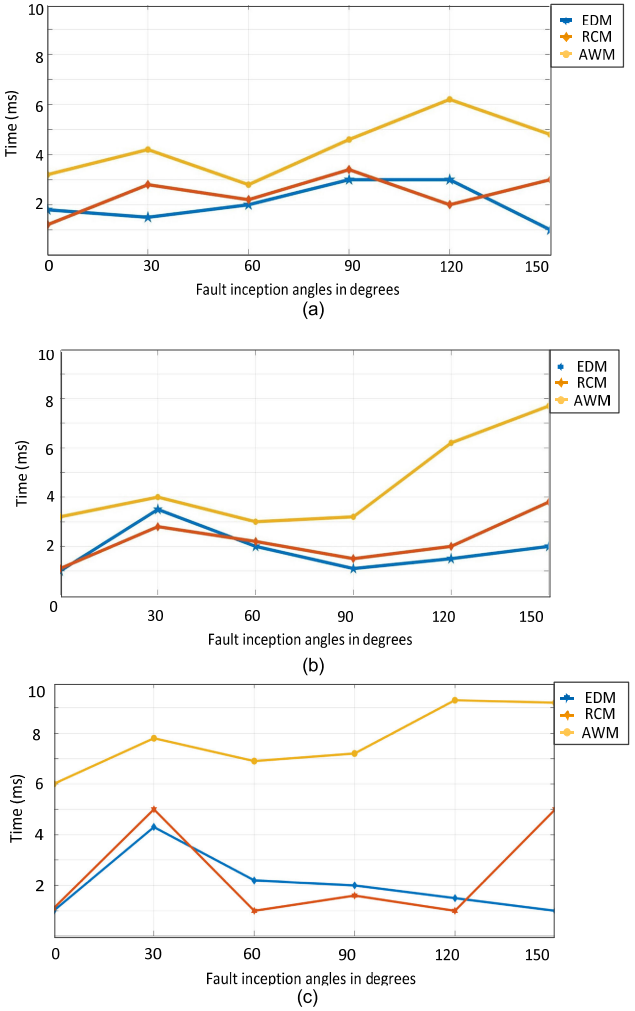

FIGURE 14. Comparison of EDM, RCM, and AWM: (a) single line-to-ground fault, (b) double line-to-ground fault, and (c) three-phase line fault.

remained unchanged. The peak fault currents, however, were slightly different, mainly due to the decrease in the lumped-sum load at L1 and L2. Changes in peak currents may result in different fault detection times for the two network topologies, as shown in Table 4.

C. COMPARATIVE ANALYSIS WITH OTHER METHODS

To verify the performance of the proposed method, two existing fault detection methods are used as benchmarks: the area waveform method (AWM) [8] and the rate of change of the current method (RCM) [9]. The AWM is mainly used to calculate the area under the three-phase current curves. For each phase, the half-cycle area was calculated and compared with the next half-cycle area. The RCM uses the differences between the current amplitudes of consecutive data points. The benchmark methods and the proposed fault detection method are defined using the MATLAB/Simulink software platform, and the same conditions were used for the simulations. The predefined threshold limits for EDM, RCM, and AWM are 200, 20, and 7, respectively [8], [9]. Fig. 14 shows the fault-detection time for different fault inception angles. It is observed that EDM provides satisfactory outputs compared with AWM and RCM at different FIAs and fault types. Additionally, the other cases were examined for all three methods. In the case of a high-impedance fault, the AWM fails to detect the fault, whereas EDM and RCM detect it. In the case of a transformer in-rush, which is a normal case, the RCM considers it as a fault. Noise introduction to the data results in false alarms by RCM, whereas other methods detect it as a safe operation. In the case of voltage imbalance, all three methods consider it to be in a normal state. The additional cases are tabulated in Table 5, where the ''red'' font specifies wrong responses and the ''green'' specifies correct responses.

TABLE 5. Comparison among existing methods.

Cases	Proposed EDM	RCM	AWM
High impedance single-line-to-ground fault	Fault detected	Fault detected	No fault detected
Transformer inrush current	No fault detected	Fault detected	No fault detected
Voltage imbalance	No fault detected	No fault detected	No fault detected
Normal case with 10% SNR noise.	No fault detected	Fault detected	No fault detected

V. CONCLUSION

In this study, the zero- and negative-sequence components of the currents were used to define a moving energy deviation matrix as the driving point for fault detection. Furthermore, an IMF selection method was defined. The analysis of various fault and normal cases shows that the proposed method performs better than the standard methods. The test results and comparison of the proposed method with other existing methods prove its reliability and efficiency.

REFERENCES

[1] O. P. Veloza and F. Santamaria, ''Analysis of major blackouts from 2003 to 2015: Classification of incidents and review of main causes,'' *Electr. J.*, vol. 29, no. 7, pp. 42–49, 2016.
[2] M. Usama, H. Mokhlis, M. Moghavvemi, N. N. Mansor, M. A. Alotaibi, M. A. Muhammad, and A. A. Bajwa, ''A comprehensive review on protection strategies to mitigate the impact of renewable energy sources on interconnected distribution networks,'' *IEEE Access*, vol. 9, pp. 35740–35765, 2021, doi: 10.1109/ACCESS.2021.3061919.
[3] F. Wang, L. Li, C. Li, Q. Wu, Y. Cao, B. Zhou, and B. Fang, ''Fractal characteristics analysis of blackouts in interconnected power grid,'' *IEEE Trans. Power Syst.*, vol. 33, no. 1, pp. 1085–1086, Jan. 2018.

[4] Y. Zhang, Z. Bao, Y. Cao, G. Li, and G. Chen, "Long-term effect of different topology evolutions on blackouts in power grid," *Int. J. Electr. Power Energy Syst.*, vol. 62, pp. 718–726, Nov. 2014.
[5] R. Yan, N.-A. Masood, T. K. Saha, F. Bai, and H. Gu, "The anatomy of the 2016 South Australia blackout: A catastrophic event in a high renewable network," *IEEE Trans. Power Syst.*, vol. 33, no. 5, pp. 5374–5388, Sep. 2018.
[6] M.-F. Guo, N.-C. Yang, and L.-X. You, "Wavelet-transform based early detection method for short-circuit faults in power distribution networks," *Int. J. Elect. Power Energy Syst.*, vol. 99, pp. 706–721, Jul. 2018.
[7] D. Guillen, M. R. A. Paternina, J. Ortiz-Bejar, R. K. Tripathy, A. Zamora-Mendez, R. Tapia-Olvera, and E. S. Tellez, "Fault detection and classification in transmission lines based on a PSD index," *IET Gener., Transmiss. Distrib.*, vol. 12, no. 18, pp. 4070–4078, Oct. 2018.
[8] R. Li, L. Xu, and L. Yao, "DC fault detection and location in meshed multiterminal HVDC systems based on DC reactor voltage change rate," *IEEE Trans. Power Del.*, vol. 32, no. 3, pp. 1516–1526, Jun. 2017.
[9] M. F. Guo, L. You, and X. Wei, "A flexible current limiting method of distribution network short circuit fault based on the voltage feedback control," *Trans. China Electrotech. Soc.*, vol. 32, no. 11, pp. 48–56, 2017.
[10] É. M. Lima, R. D. A. Coelho, N. S. D. Brito, and B. A. D. Souza, "High impedance fault detection method for distribution networks under nonlinear conditions," *Int. J. Electr. Power Energy Syst.*, vol. 131, Oct. 2021, Art. no. 107041.
[11] F. P. Souza, L. F. Q. Silveira, F. B. Costa, and M. M. Leal, "High-impedance fault identification using cyclostationary characteristic analysis," *Electr. Power Syst. Res.*, vol. 195, Jun. 2021, Art. no. 107150.
[12] M. Wei, W. Liu, H. Zhang, F. Shi, and W. Chen, "Distortion-based detection of high impedance fault in distribution systems," *IEEE Trans. Power Del.*, vol. 36, no. 3, pp. 1603–1618, Jun. 2021.
[13] J. D. R. Penaloza, A. Borghetti, F. Napolitano, F. Tossani, and C. A. Nucci, "Performance analysis of a transient-based earth fault protection system for unearthed and compensated radial distribution networks," *Electr. Power Syst. Res.*, vol. 197, Aug. 2021, Art. no. 107306.
[14] C. Tsiafis, I. Tsiafis, M. Xanthopoulou, and P. Todorovic, "Fault detection and determination in ball bearing based on EMD and marginal spectral analysis," *J. Balkan Tribol. Assoc.*, vol. 21, no. 4, pp. 982–990, 2015.
[15] Y. Jiang, C. Tang, X. Zhang, W. Jiao, G. Li, and T. Huang, "A novel rolling bearing defect detection method based on bispectrum analysis and cloud model-improved EEMD," *IEEE Access*, vol. 8, pp. 24323–24333, 2020.
[16] M.-F. Guo, N.-C. Yang, and W.-F. Chen, "Deep-learning-based fault classification using Hilbert–Huang transform and convolutional neural network in power distribution systems," *IEEE Sensors J.*, vol. 19, no. 16, pp. 6905–6913, Aug. 2019.
[17] S. Cho, M. R. Shahriar, and U. Chong, "Identification of significant intrinsic mode functions for the diagnosis of induction motor fault," *J. Acoust. Soc. Amer.*, vol. 136, no. 2, pp. EL72–EL77, Aug. 2014.
[18] H. Yang, S. Liu, and H. Zhang, "Adaptive estimation of VMD modes number based on cross correlation coefficient," *J. Vibroeng.*, vol. 19, no. 2, pp. 1185–1196, Mar. 2017.
[19] P. S. Kumar, L. A. Kumaraswamidhas, and S. K. Laha, "Selecting effective intrinsic mode functions of empirical mode decomposition and variational mode decomposition using dynamic time warping algorithm for rolling element bearing fault diagnosis," *Trans. Inst. Meas. Control*, vol. 41, no. 7, pp. 1923–1932, Apr. 2019.
[20] Z. Zhang, P. Tang, and T. Corpetti, "Time adaptive optimal transport: A framework of time series similarity measure," *IEEE Access*, vol. 8, pp. 149764–149774, 2020.
[21] Y. Rubner, C. Tomasi, and L. J. Guibas, "The earth mover's distance as a metric for image retrieval," *Int. J. Comput. Vis.*, vol. 40, no. 2, pp. 99–121, Nov. 2000.
[22] J. Xu, Z. Zhang, A. K. H. Tung, and G. Yu, "Efficient and effective similarity search over probabilistic data based on earth mover's distance," *VLDB J.*, vol. 21, no. 4, pp. 535–559, Aug. 2012.
[23] M. A. Maldonado, G. S. Torres, and J. W. Branch, "Registration of range images using a histogram based metric," *Dyna*, vol. 79, no. 176, pp. 27–34, Dec. 2012.
[24] J. W. Li, Y. H. Wang, and T. N. Tan, "Video-based face recognition using earth mover's distance," in *Audio and Video Based Biometric Person Authentication*, vol. 3546, T. Kanade, A. Jain, and N. K. Ratha, Eds. Berlin, Germany: Springer, 2005, pp. 229–238.
[25] N. E. Huang, Z. Shen, S. R. Long, M. C. Wu, H. H. Shih, Q. Zheng, N.-C. Yen, C. C. Tung, and H. H. Liu, "The empirical mode decomposition and the Hilbert spectrum for nonlinear and non-stationary time series analysis," *Proc. Roy. Soc. London A, Math., Phys. Eng. Sci.*, vol. 454, no. 1971, pp. 903–995, Mar. 1998.
[26] R. W. Komm, F. Hill, and R. Howe, "Empirical mode decomposition and Hilbert analysis applied to rotation residuals of the solar convection zone," *Astrophys. J.*, vol. 558, no. 1, pp. 428–441, Sep. 2001.
[27] L. Mengting, H. Darong, Z. Ling, C. Ruyi, F. Kuang, and J. Yu, "An improved fault diagnosis method based on a genetic algorithm by selecting appropriate IMFs," *IEEE Access*, vol. 7, pp. 60310–60321, 2019.
[28] H. Huang and B. Natalie, "Bearing vibration data collected under time-varying rotational speed conditions," *Data Brief*, vol. 21, pp. 1745–1749, 2018.
[29] I. E. Commission, *Electromagnetic Compatibility (EMC)-Limits-Assessment of Emission Limits for the Connection of Unbalanced Installations to MV, HV and EHV Power Systems*, document TR IEC/TR 61000-3-13, 2012.
[30] N. E. M. Association, "Motors and generators," Nat. Elect. Manufacturers Assoc., Standards Publication, USA, 2009.
[31] F. Ghassemi and M. Perry, "Review of voltage unbalance limit in the GB grid code CC.6.1.5 (b)," Nat. Grid, Sindlesham, U.K., Tech. Rep., 2014, pp. 14–58.

NIEN-CHE YANG was born in Keelung, Taiwan, in 1977. He received the B.S., M.S., and Ph.D. degrees from the National Taiwan University of Science and Technology, Taipei, Taiwan, in 2002, 2004, and 2010, respectively, all in electrical engineering. Since 2018, he has been with the Faculty Member of the National Taiwan University of Science and Technology, where he is currently an Associate Professor of Electrical Engineering. His research interests include micro-grid state estimation, harmonic three-phase power flow analysis, probabilistic three-phase power flow analysis, energy loss computation in low voltage networks, micro-grid, smart grid, and electric vehicle. He is a member of the Phi Tau Phi Scholastic Honor Society.

ABHILASH SEN received the master's degree from the National Institute of Technology Meghalaya, India, in 2019. He is currently pursuing the Ph.D. degree in electrical engineering from the National Taiwan University of Science and Technology, Taipei, Taiwan. His research interests include electrical fault analysis, distribution networks, renewable systems, and deep learning applications.